Single- and double-electron capture cross sections for slow He^{2+} impact on O_2, H_2, and D_2

S. Figueira da Silva, HP. Winter, and F. Aumayr*
Institut für Allgemeine Physik, TU Wien, Wiedner Haupstrasse 8-10/E134, A-1040 Vienna, Austria
(Received 2 February 2007; published 13 April 2007)

Single- and double-electron capture cross sections have been measured for He^{2+} impact on O_2, H_2, and D_2 at impact energies smaller than 2 keV/amu. The method applied combines the collection of slow product ions and electrons with primary ion-beam attenuation and stopping in a differentially pumped target gas chamber. Comparison with previous experimental and theoretical results is made. For He^{2+} collisions with H_2 we find that double-electron capture is more important than single-electron capture below 0.2 keV/amu. This result is also confirmed by cross-section measurements for He^{2+} on D_2.

DOI: 10.1103/PhysRevA.75.042706 PACS number(s): 34.50.−s, 34.70.+e, 39.90.+d

I. INTRODUCTION

In future burning deuterium-tritium (D-T) fusion plasmas the resulting He ash will be the most important impurity species. Accurate knowledge of charge-transfer collision cross sections involving doubly ionized helium (He^{2+}, i.e., α particles) and molecules present in the colder outer region of the plasma is of critical importance for plasma modeling as well as for helium ash removal from the divertor region of fusion devices [1]. Helium is also the second most abundant element in the universe and is part of the solar wind. Interactions of He^{2+} with molecules like H_2, O_2, and CO have recently gained a lot of interest due to the observation of soft x-ray emission from comets which have been interpreted as being due to charge exchange between multiply charged ions of the solar wind and cometary atmosphere [2,3]. Moreover, such processes are of relevance for many applied fields including ion implantation, thin film manufacturing, and biological studies.

In charge-exchange processes of He^{2+} colliding with O_2, cross-section data are still scarce in the literature and no systematic theoretical work has been carried out. Ishii *et al.* [4] reported single-electron capture (SEC) and double-electron capture (DEC) cross sections for He^{2+}-O_2 collisions at low impact energy where they showed that the DEC cross section appears to dominate the SEC cross section below 100 eV/amu. Okuno *et al.* [5] studied the DEC processes of He^{2+} on O_2 collisions by means of a double coincidence time-of-flight spectroscopy where they identified the exit channels with respective branching rations. Recently Kusakabe *et al.* [6] presented single- and double-electron capture cross sections for He^{2+} impact on various molecular targets (among them O_2 and H_2) in the energy range from 0.6 to 2.7 keV/amu. Other experimental investigations of the He^{2+}-O_2 collision system have been concerned mainly with the measurements of state selective single-electron capture by means of translational energy spectroscopy (TES) [7–11].

For charge-exchange processes of He^{2+} with H_2 molecules quite a few numbers of experimental data [6,7,12–19] and theoretical results [20–23] have been published earlier at intermediate and low impact energy, but for ion impact energy <1 keV/amu results remain inconclusive. Measurements by Shah and Gilbody [24] and Kusakabe *et al.* [16] of SEC and DEC processes above 1 keV/amu showed that SEC is dominant by about an order of magnitude in the cross section. The measurement of the same processes at low energies by Okuno *et al.* [18] has indicated that the DEC cross section dominates the SEC cross section. Shimakura *et al.* [22] studied theoretically SEC and DEC processes in the energy range from 17 eV/amu to 0.67 keV/amu based on a molecular orbital expansion method and showed that the calculated DEC cross section values indeed exceed the SEC data points below 100 eV/amu. Recently Kusakabe *et al.* [6] presented their experimental SEC and DEC cross sections in the energy range from 0.6 to 2.7 keV/amu, where they found that SEC is the dominant reaction and that the DEC cross sections have a nearly constant value at their impact energy range. The same conclusion was also found for He^{2+} on O_2 collision systems.

In the present work, an experimental setup has been constructed and utilized for measuring absolute cross sections for single- (SEC) and double-electron capture (DEC) in collisions of slow singly and multiply charged ions with gaseous atoms and molecules. Our technique combines a collection of slow product ions with primary ion-beam attenuation and stopping in a differentially pumped target gas chamber, where the pressure is measured by an absolutely calibrated capacitance manometer. The reliability of our experimental setup was first checked by proof-of-principle measurements in comparison with well-established SEC and DEC cross sections for impact of slow doubly charged noble gas ions on their respective atoms (He, Ne, Ar) [25], where resonant DEC is the clearly dominant reaction. Additionally, measurements of SEC and DEC for He^{2+} collisions with Ne were carried out, a system for which SEC is expected to proceed, at low impact energy, via a single channel only [25]. In the present work, we have systematically measured SEC and DEC cross sections for He^{2+} impact on O_2, H_2, and D_2 at impact energies smaller than 2 keV/amu.

II. EXPERIMENTAL TECHNIQUE

A. Experimental setup

The projectile ion beam is generated by means of a 14.5 GHz electron cyclotron resonance ion source (ECRIS) ion source which is described in [26]. Basically, the source

*Electronic address: aumayr@iap.tuwien.ac.at

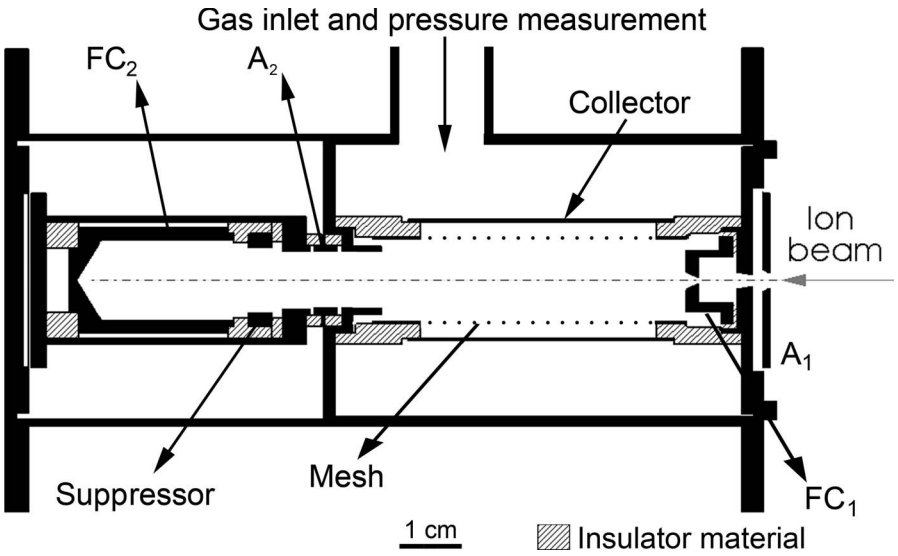

FIG. 1. Schematic view of the charge-exchange experiment. First aperture (A_1) with 2.5 mm diameter opening, Faraday cup for incoming current normalization (FC_1) with 1.0 mm aperture, insulated second aperture (A_2) for final ion selection with 10 mm diameter aperture. FC_2 serves for attenuated ion current measurement.

consists of a set of four permanent magnet rings and a Halbach-type hexapole providing the magnetic field for plasma confinement. The plasma heating is done by injection of microwaves with a total power of up to 350 W in the frequency range of 12.7 to 14.5 GHz. The ions are extracted by a potential applied to the ion source corresponding to ion acceleration voltages between 1 and 10 kV. The extracted ion beam is focused by a magnetic quadrupole system and then mass-to-charge analyzed by a 60° sector magnet.

Before traveling to the charge-exchange apparatus, the beam is steered horizontally and vertically by a first set of deflection plates and collimated by an aperture of 2.5 mm diameter. This aperture is mounted electrically insulated such that the ion-beam current can be monitored. A second set of deflection plates can be used to guide the ion beam into a set of four cylindrical electrostatic lenses for focusing and deceleration.

The collision chamber is schematically shown in Fig. 1. An insulated aperture (A_1) of 2.5 mm diameter at the chamber entrance serves for monitoring the incoming ion-beam current. Inside the chamber is a first Faraday cup (FC_1) with 1 mm aperture for normalizing the ion current measured in the second Faraday cup (FC_2) to the incoming ion current. The collision region is covered by a meshed cylinder and a slow particle collector. Behind the collision region an insulated aperture A_2 is used for discriminating primary singly charged ions produced by SEC from doubly charged ions by applying a retarding potential, i.e., the incident doubly charged ions are completely reflected and only the charge-exchanged (single-charged) ions can reach the Faraday cup FC_2 (see Sec. II B 2). With a 10 mm diameter the A_2 aperture accepts a mean scattering angle of ±8°. Subsequent to A_2 a suppressor ring is biased negatively with respect to the subsequent Faraday cup FC_2 in order to keep secondary electrons in FC_2 where the attenuated ion current is measured. The background pressure of our setup is in the lower 10^{-8} mbar range. The total pressure in the gas cell is measured absolutely by a calibrated capacitance manometer (Baratron). In order to assure single-collision conditions typical target gas pressures are in the range of 10^{-4} to 10^{-3} mbar and the purity of the target is monitored by a partial pressure gauge.

As mentioned previously, the projectile ions are extracted by the potential U_{accel} applied to the ion source between 1 and 10 kV. The initial kinetic energy of the primary beam is given by

$$E_i = qU_{\text{accel}}, \tag{1}$$

where E_i is the primary ion initial kinetic energy and q is the ion charge. Considering the extraction of doubly charged ions ($q=2$), the impact energy collision range down to 2000 eV was mainly defined by changing the potential applied to the ion source. For lower impact energy, the incoming ion beam was decelerated by means of appropriate potentials applied to the gas cell. The final impact energy is therefore defined by

$$E_f = q(U_{\text{accel}} - U_{\text{dec}}), \tag{2}$$

where U_{dec} is the deceleration potential applied to the gas cell. U_{dec} is the reference potential for the other components of the charge-exchange system. The plate A_1, Faraday cup for normalization (FC_1), meshed cylinder, plate A_2, and the Faraday cup for current measurement (FC_2) were biased at the same potential as the gas cell. The suppressor was biased always negatively with respect to the potential applied to the gas cell ($U_{\text{dec}}-50$ V) in order to keep secondary electrons in the last Faraday cup. The collector was biased either slightly positively or negatively with respect to U_{dec} depending on the requirement that electrons or ions should be collected. Five picoammeters were used to measure the various currents (FC_1, FC_2, A_1, A_2, and collector). In order to be able to apply a high voltage to these picoammeters they were operated via insulating transformers. The output signal (proportional to the measured current) was connected to the data acquisition system via galvanic insulating.

B. Cross-section determination

In this work, the charge transfer reactions were identified by analysis of *fast* projectile and *slow* product ions, and ad-

ditionally by measuring the slow electrons produced during the collisions. At low impact energies ($v \ll 1$ a.u.), the following processes are expected during collisions of He^{2+} ions with diatomic molecules A_2:

$$He^{2+} + A_2 \rightarrow He^{(2-t)+} + [A_2]^{r+} + (r-t)e^-. \quad (3)$$

Capture of t electrons by the projectile leads to single- ($t=1$) and double- ($t=2$) electron capture. After the collision, the target molecule $[A_2]^{r+}$ can be in several different states including dissociative ones.

If $t \neq r$, "transfer ionization" occurs in which $(r-t)$ electrons are ejected. The cross sections associated to these reactions were obtained by a combination of different techniques, as outlined in the next section.

1. Beam attenuation measurement

In our setup the current of fast primary He^{2+} as well as He^+ product ions are measured in FC_2. Under single-collision conditions the decrease of the doubly charged-ion current and the related increase of the singly charged-ion current as function of small target thickness π leads to a total attenuated current of

$$I_{FC}(\pi) = I_0 \exp\left[-\left(\sigma_{20} + \frac{\sigma_{21}}{2}\right)\pi\right] \approx I_0\left[1 - \left(\sigma_{20} + \frac{\sigma_{21}}{2}\right)\pi\right], \quad (4)$$

where I_0 is the primary ion current measured in FC_2 without attenuation, and σ_{20} and σ_{21} are the double- (DEC) and single- (SEC) electron capture cross sections, respectively. Single collisions are assured as long as $\sigma\pi \ll 1$.

2. Retarding-field measurement

After traversing the target gas cell, fast primary He^{2+} and charge-exchanged He^+ ions can be separated by a suitable retarding field. For an initial ion-acceleration voltage U_{accel} the primary ions will be reflected by a slightly higher retarding potential, while ions that have captured one electron can only be reflected by a higher potential ($U_R \geq 2U_{accel}$). The SEC cross section can thus be obtained from the separated current of fast singly charged He^+ ions measured under retarding conditions

$$I_{FC}(\pi) = I_0 \exp(\sigma_{21}\pi) \approx I_0\sigma_{21}\pi, \quad (5)$$

with σ_{21} being the SEC cross section. Once σ_{21} is known, σ_{20} can be evaluated from the results obtained from the attenuation measurements [Eq. (4)].

3. Collection of slow ions and electrons

Slow charged secondary particles (A_2^+, A^+, e^-) are measured on a cylindrical electrode surrounding the collision region and shielded by a highly transparent mesh. We distinguish between slow ions and electrons by means of the potential applied to the collector with respect to the meshed cylinder. The dependence of slow ions measured on the collector (biased negatively) as function of π is given by

$$I^+_{coll}(\pi) = \varepsilon I_0 \exp(\sigma_+\pi) \approx \varepsilon I_0\sigma_+\pi, \quad (6)$$

where σ_+ is the production cross section for slow ions and ε the transparency factor ($0 \leq \varepsilon \leq 1$) of the mesh in front of the collector electrode. The measurements of slow ions are directly correlated to the attenuated current and are used as a cross check considering charge conservation [19]. The factor ε takes into account the mesh design (coiled 0.1 mm molybdenum wire with 2 mm separation of each turn, corresponding to 98% transparency, and the support rods of the inner cylinder on which the mesh is fixed). We have determined ε from well-established resonant SEC cross sections for Ar^+, Ne^+, and He^+ impact (for details see [25]). ε turned out to be constant for a wide range of ion species, impact energies, and target gas pressure, resulting in a value of $\varepsilon = 0.46 \pm 0.02$.

The increase of the slow electron current measured on the collector (if biased positively) as function of target thickness π is given by

$$I^-_{coll}(\pi) \approx -\varepsilon I_0 \frac{\sigma_{TI}}{2}\pi, \quad (7)$$

where σ_{TI} is the transfer ionization cross section.

III. RESULTS AND DISCUSSIONS

Collisions of He^{2+} on O_2 and H_2 were carried out at ion impact energies below 2000 eV/amu. The final impact energies were defined by both the potential applied to the ion source and the deceleration voltage applied to the gas cell. In order to check the influence of electrostatic lenses at low impact energies, several different combinations of the source and deceleration voltages leading to the same impact energy were applied but no systematic difference between the results was found. Our measured cross sections for SEC and DEC are given in Tables I and II, and shown in Figs. 2–5.

The associated error bars give the absolute errors. In the worst case the absolute errors were estimated to be about 20% [25].

A. O_2 target

For the impact energy range investigated in this work, it is expected that the following processes are most important during single collisions of He^{2+} with O_2 molecules:

Nondissociative SEC

$$He^{2+} + O_2 \rightarrow He^+(n=2) + O_2^+(\Delta E = 1.3 \text{ eV}), \quad (8)$$

Dissociative SEC

$$He^{2+} + O_2 \rightarrow He^+(n=1) + O_2^{+*} \text{ (many dissociative states)}, \quad (9)$$

Dissociative DEC

$$He^{2+} + O_2 \rightarrow He + O^+ + O^+, \quad (10)$$

$$He^{2+} + O_2 \rightarrow He + O^{2+} + O, \quad (11)$$

Dissociative DEC with ionization

$$He^{2+} + O_2 \rightarrow He + O^{2+} + O^+ + e^-. \quad (12)$$

TABLE I. Single- (σ_{21}) and double- (σ_{20}) electron capture cross sections of He^{2+} ions colliding with O_2 molecular targets.

	O_2	
E (keV/amu)	σ_{21} (10^{-16} cm^2)	σ_{20} (10^{-16} cm^2)
0.0035	0.95	8.07
0.0066	1.68	6.23
0.0100	1.64	6.74
0.0200	2.35	5.10
0.0500	3.02	4.92
0.0666	3.42	4.29
0.1000	3.54	3.79
0.2500	5.38	3.97
0.3330	5.92	4.26
0.5000	6.10	4.09
0.6660	7.44	3.43
1.0000	7.83	3.33
1.3330	8.14	3.41
1.5000	8.22	3.49
2.0170	9.12	3.10

The processes (10)–(12) were identified by means of double coincidence time-of-flight [5] at 1 keV/amu impact energy with 78%, 9.9%, and 12% branching ratios, respectively. The process (8) represents the nondissociative single-electron capture into $n=2$ states of He^+ with production of O_2^+ in the ground state ($X\,^2\Pi_g$). Process (9) has a rather broad energy gain ($6<\Delta E<10$ eV) and represents the dissociative single-electron capture into $n=1$ state of He^+ with production of O_2^+ in several excited states [7–9].

In our setup we are only able to distinguish between SEC [process (8)+(9)] and DEC [process (10)+(11)+(12)]. The measured cross sections are shown in Figs. 2 and 3 as functions of impact energy. The measurements were not only performed with $^4He^{2+}$ but also with $^3He^{2+}$ isotopes in order to check whether possible impurity ions with the same mass to charge ratio (e.g., H_2^+) as $^4He^{2+}$ influence to the measured signals. The cross section results for both isotope projectiles agree very well, which indicates that the contribution from H_2^+ projectiles is of no relevance. This observation has also been made before for the collision system $^4He^{2+}$ and $^3He^{2+}$ on Ne [25].

TABLE II. Single- (σ_{21}) and double- (σ_{20}) electron capture cross sections of He^{2+} ions colliding with H_2 molecular targets.

	H_2	
E (keV/amu)	σ_{21} (10^{-16} cm^2)	σ_{20} (10^{-16} cm^2)
0.013	0.53	4.82
0.033	0.97	3.09
0.067	1.12	2.71
0.167	2.10	1.45
0.333	2.38	1.08
0.667	2.64	0.72
1.000	2.68	0.68
1.333	2.88	0.47
2.000	2.80	0.33

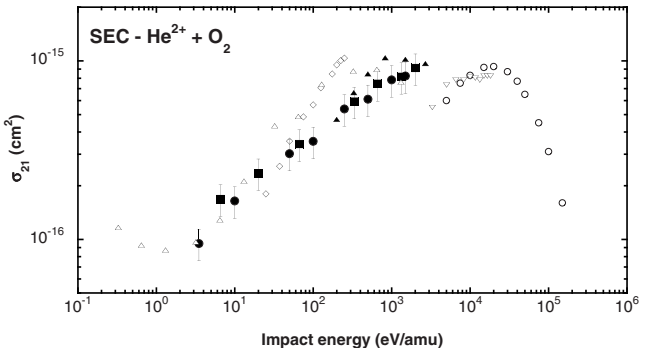

FIG. 2. Single-electron capture cross section for $^4He^{2+}$ and $^3He^{2+}$ on O_2 collisions as a function of impact energy. Full circles—this work ($^4He^2$ projectile), full squares—this work ($^3He^2$ projectile), full triangles—Kusakabe *et al.* [6], open diamonds—Kamber *et al.* [8], open triangles—Ishii *et al.* [4], open circles—Rudd *et al.* [19], inverted open triangles—Shah and Gilbody [24].

As far as SEC cross sections are concerned, the present results are in reasonably good agreement with previous measurements, although we could neither reproduce the trend presented by Ishii *et al.* [4] nor Kamber *et al.* [8]. The SEC cross section increases with increasing incident energy and unfortunately the connection with data for impact energies above 5 keV/amu is still not clear yet (see Fig. 2).

In the impact energy range from 0.2 to 2 keV/amu our data for the DEC cross section agree very well with earlier experimental results. For impact energies below 0.2 keV/amu our cross sections increase as the collision energy decreases. This is in qualitative agreement with results of Ishii *et al.* [4], but these authors obtained higher values for the DEC cross sections. A possible explanation for this dif-

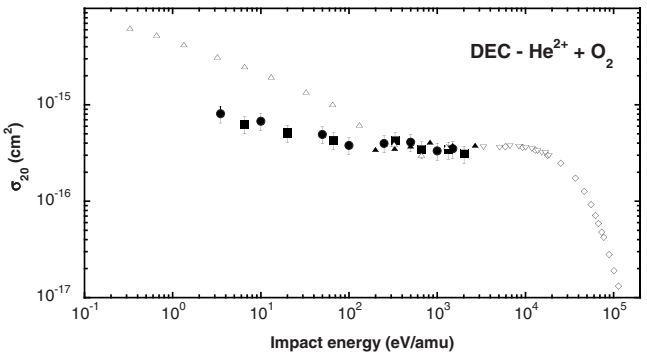

FIG. 3. Double electron capture cross section for $^4He^{2+}$ and $^3He^{2+}$ on O_2 collisions as a function of impact energy. Full circles—this work ($^4He^2$ projectile), full squares—this work ($^3He^2$ projectile), full triangles—Kusakabe *et al.* [6], open triangles—Ishii *et al.* [4], open diamonds—Rudd *et al.* [19], inverted open triangles—Shah and Gilbody [24].

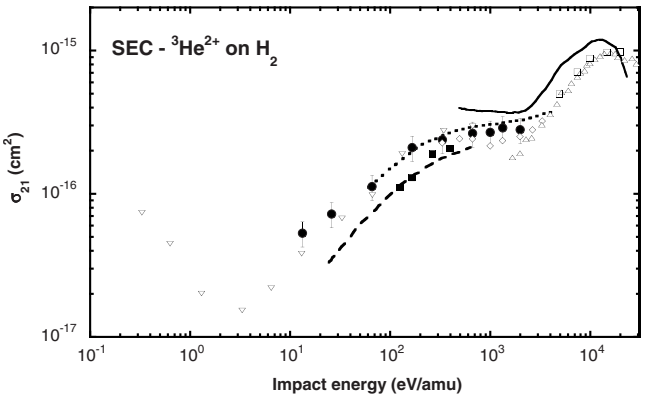

FIG. 4. Single-electron capture cross section for $^3He^{2+}$ on H_2 collisions as function of impact energy. Experimental results: full circles—this work, full squares—Kusakabe *et al.* [6], open diamonds—Kusakabe *et al.* [16], open inverted triangles—Okuno *et al.* [18], open squares—Rudd *et al.* [19], open triangles—Shah and Gilbody [24]. Theoretical results: full lines—Errea *et al.* [20], dashed line—Shimakura and Kimura [22], dotted line—Kusakabe *et al.* [6].

ference could be the limited acceptance angle of their experiment leading to an artificial increase of beam current attenuation with decreasing impact energy. Our apparatus, on the contrary, is designed to accept scattering angles up to ±8°.

B. H_2 and D_2 targets

In the low impact energy range the following processes are most relevant in He^{2+}-H_2 and -D_2 collisions:

$$\text{DEC} \quad He^{2+} + H_2 \rightarrow He + H^+ + H^+, \tag{13}$$

$$\text{SEC-ND} \quad He^{2+} + H_2 \rightarrow He^+ + H_2^+, \tag{14}$$

$$\text{SEC-D} \quad He^{2+} + H_2 \rightarrow He^+ + H^+ + H, \tag{15}$$

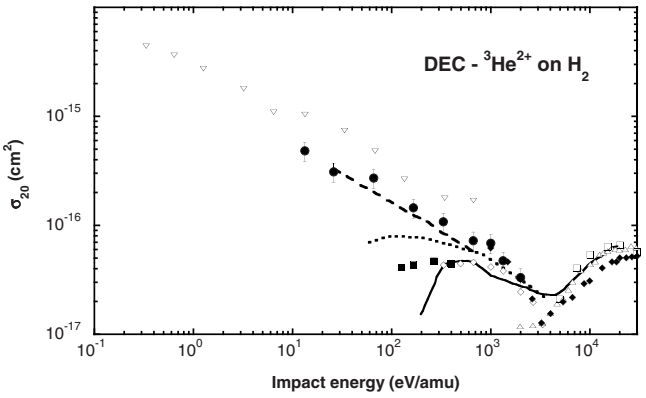

FIG. 5. Double-electron capture cross section for $^3He^{2+}$ on H_2 collisions as function of impact energy. Experimental results: full circles—this work, full squares—Kusakabe *et al.* [6], open diamonds—Kusakabe *et al.* [16], open inverted triangles—Okuno *et al.* [18], open squares—Rudd *et al.* [19], full diamonds—Afrosimov *et al.* [27], open triangles—Shah and Gilbody [24]. Theoretical results: full lines—Errea *et al.* [20], dashed line—Shimakura and Kimura [22], dotted line—Kusakabe *et al.* [6].

$$\text{SEC-TI} \quad He^{2+} + H_2 \rightarrow He^+ + 2H^+ + e^-. \tag{16}$$

The double-electron capture process (DEC) [Eq. (13) and associated cross section σ_{20}] resulted in target dissociation via Coulomb explosion. Process (14) is the nondissociative single-electron capture (SEC-ND) leading to the formation of He^{2+} $(n=2)$ with a minimum endothermic energy defect of about −1.8 eV, which can be broadened due to vibrational excitation $(v=0 \rightarrow \infty)$ of the H_2^+ molecular product ions [14]. The dissociative single-electron capture (SEC-D) reaction [process (15)] also carries a broad defect energy associated to the limits of Franck-Condon transitions from the H_2 $^1\Sigma_g$ ground state to repulsive states of H_2^+ leading to $H^+ + H(2s)$ and $H^+ + H(2p)$ products [7,14]. Process (16) describes single-electron capture with target excitation followed by electron ejection (SEC-TI) which is possible to form a large number of dissociative H_2^{+*} states. At our low impact energies the SEC-TI reaction channels prefer considerably small exothermic energy defects (typically $\Delta E = 5$ eV [7]).

The present experimental cross sections for SEC and DEC of $^3He^{2+}$ colliding with H_2 as function of impact energy are shown in Figs. 4 and 5, respectively. In contrast to the O_2 target, only $^3He^{2+}$ ions were used as projectiles because back diffusion of H_2^+ from the gas cell into our ECRIS was observed.

The present SEC cross section results are found to be in agreement with Okuno *et al.* [18] and connect smoothly to Kusakabe *et al.* [16] and Shah and Gilbody [24]. We note that the present SEC cross sections are in excellent agreement with the close-coupling calculation of Kusakabe *et al.* [6].

For the DEC cross section experimental and theoretical results are in reasonable agreement above 1 keV/amu impact energy. For lower impact energies considerable deviations occur. Okuno *et al.* [18] found that the DEC cross section has a monotonic upward trend as impact energies decrease and dominates over the SEC cross section for lower impact energies. The theoretical work of Shimakura *et al.* [22] based on a molecular orbital expansion method supports this trend by showing that indeed the calculated DEC cross section values exceed the SEC data below 100 eV/amu. The experimental results presented by Kusakabe *et al.* [6,16] on the other hand have shown that DEC cross section values do not exceed the SEC cross section. They even report a plateau in the range of 0.13–0.8 keV/amu for the DEC cross section, which is to some extent also supported by their close-coupling calculations. The present DEC cross section data for $^3He^{2+}$ on H_2 collisions are compared in Fig. 5. Our DEC cross sections increase monotonically as the impact energy decreases and exceed the SEC data for energies below 100 eV/amu. Our data are in very good agreement with the theory by Shimakura *et al.* [22] and closely follow the trend of the data by Okuno *et al.*, whose absolute cross section values are about a factor of 2 higher. Again a possible reason for this difference could be the small acceptance angle of their experiment, as discussed before.

Our DEC cross sections obtained via attenuation methods (Secs. II B 1 and II B 2) are in excellent agreement with

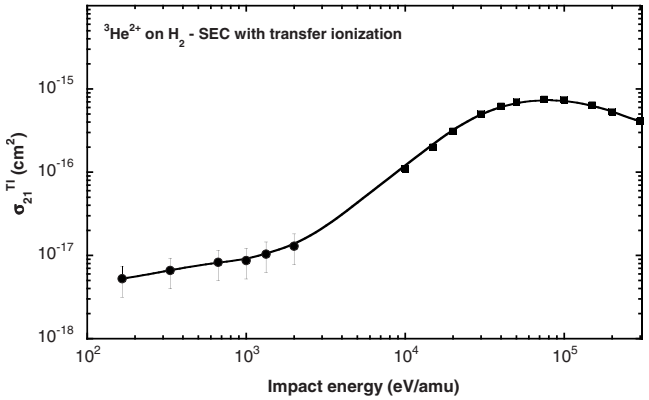

FIG. 6. Transfer ionization cross section [process (16)] for $^3He^{2+}$ on H_2 collisions as function of impact energy. Full circles—present work, full squares—Rudd *et al.* [19].

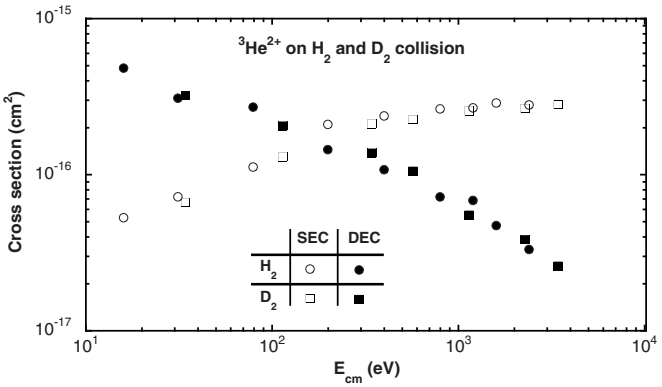

FIG. 7. SEC and DEC cross sections for $^3He^{2+}$ on D_2 compared to $^3He^{2+}$ on H_2 collisions as function of impact energy in center-of-mass system. SEC: open circles—H_2 target, open squares—D_2 target. DEC: full circles—H_2 target, full squares—D_2 target.

DEC cross sections derived from slow ion collection (Sec. II B 3). In addition, the transfer ionization cross section (σ_{TI}) obtained by measurement of slow electrons [Eq. (7)] has been determined and is shown in Fig. 6. The σ_{TI} cross section for transfer ionization [reaction (16)] increases with increasing impact energy and can be smoothly connected to the measurement by Rudd *et al.* [19].

We have also carried out additional measurements for $^3He^{2+}$-D_2 collisions. D_2 was used since the electronic processes are expected to be identical to those in H_2 targets but the heavier isotope provides kinematic differences, e.g., projectile scattering with a larger laboratory angle. The SEC and DEC cross sections for $^3He^{2+}$ on D_2 compared to $^3He^{2+}$ on H_2 collisions as a function of impact energy in the center-of-mass system are shown in Fig. 7. We do not observe any systematic changes between both results and therefore we conclude that our apparatus collects practically all product ions during the collisions even for higher scattering angles.

IV. SUMMARY

We have measured single- and double-electron capture cross sections for He^{2+} colliding with O_2, H_2, and D_2. For all molecular targets investigated in this work the single-electron capture cross sections increase slowly as the collision energy increases, while the opposite trend is observed for the double-electron capture cross sections. For H_2 and D_2 targets the double-electron capture cross section exceeds the single-electron capture for impact energies below 100 eV/amu, attributed to a fact that could become of considerable importance for the removal of He ash in future burning D-T plasmas. The large cross sections for double-electron capture at low energies can be attributed to the existence of outgoing channels with favorable (small) energy defects.

ACKNOWLEDGMENTS

The present work has been supported by the Austrian Academy of Sciences (Project No. KKKOe 1-2005) and was carried out within the Association EURATOM-OEAW (Project No. P2).

[1] R. Hoekstra, D. Bodewits, S. Knoop, R. Morgenstern, L. Mendez, L. F. Errea, C. Illecas, A. Macias, B. Pons, A. Riera, F. Aumayr, and HP. Winter, *Atomic and Plasma-Material Interaction Data for Fusion* (International Atomic Energy Agency, Vienna, in press).
[2] V. Izmodenov, Y. Malama, G. Gloeckler, and J. Geiss, Astron. Astrophys. **414**, L29 (2004).
[3] D. Bodewits, R. Hoekstra, B. Seredyuk, R. W. McCullough, G. H. Jones, and A. G. G. M. Tielens, Astrophys. J. **642**, 593 (2006).
[4] K. Ishii, K. Okuno, and N. Kobayashi, Phys. Scr., T **T80**, 176 (1999).
[5] K. Okuno, T. Kaneyasu, K. Ishii, M. Yoshino, and N. Kobayashi, Phys. Scr., T **T80**, 173 (1999).
[6] T. Kusakabe, Y. Miyamoto, M. Kimura, and H. Tawara, Phys. Rev. A **73**, 022706 (2006).
[7] M. Albu, F. Aumayr, and HP. Winter, Int. J. Mass. Spectrom. **233**, 239 (2004).
[8] E. Y. Kamber, O. Abu-Haija, and S. M. Ferguson, Phys. Rev. A **65**, 062717 (2002).
[9] S. J. Martin, J. Stevens, and E. Pollack, Phys. Rev. A **43**, 3503 (1991).
[10] R. W. McCullough, T. K. McLaughlin, T. Koizumi, and H. B. Gilbody, J. Phys. B **25**, L193 (1992).
[11] W. R. Thompson, M. B. Shah, and H. B. Gilbody, Phys. Scr., T **T73**, 214 (1997).
[12] R. A. Baragiola and I. B. Nemirovsky, Nucl. Instrum. Methods **110**, 511 (1973).
[13] J. E. Bayfield and G. A. Khayrallah, Phys. Rev. A **11**, 920 (1975).
[14] J. M. Hodgkinson, T. K. McLaughlin, R. W. McCullough, J. Geddes, and H. B. Gilbody, J. Phys. B **28**, L393 (1995).

[15] R. Hoekstra, H. O. Folkerst, J. P. M. Beijers, R. Morgenstern, and F. J. de Heer, J. Phys. B **27**, 2021 (1994).
[16] T. Kusakabe, Y. Yoneda, Y. Mizumot, and K. Katsurayama, J. Phys. Soc. Jpn. **59**, 1218 (1990).
[17] W. L. Nutt, R. W. McCullough, K. Brady, M. B. Shah, and H. B. Gilbody, J. Phys. B **11**, 1457 (1978).
[18] K. Okuno, K. Soejima, and Y. Kaneko, J. Phys. B **25**, L105 (1992).
[19] M. E. Rudd, R. D. DuBois, L. H. Toburen, C. A. Ratcliffe, and T. V. Goffe, Phys. Rev. A **28**, 3244 (1983); M. E. Rudd, T. V. Goffe, and A. Itoh, *ibid.* **32**, 2128 (1985).
[20] L. F. Errea, A. Macías, L. Méndez, B. Pons, and J. Riera, J. Phys. B **36**, L135 (2003).
[21] B. C. Saha, N. F. Lane, and M. Kimura, Phys. Rev. A **44**, R1 (1991).
[22] N. Shimakura, M. Kimura, and N. F. Lane, Phys. Rev. A **47**, 709 (1993).
[23] R. Shingal and C. D. Lin, Phys. Rev. A **40**, 1302 (1989).
[24] M. B. Shah and H. B. Gilbody, J. Phys. B **11**, 121 (1978).
[25] S. Figueira da Silva, G. Kowarik, F. Aumayr, and HP. Winter, J. Phys.: Conf. Ser. **58**, 181 (2007).
[26] E. Galutschek, R. Trassl, E. Salzborn, F. Aumayr, and HP. Winter, J. Phys.: Conf. Ser. **58**, 395 (2007).
[27] V. V. Afrosimov, G. A. Leiko, and M. N. Panov, Sov. Phys. Tech. Phys. **25**, 313 (1980).